Dynamic Deformation of Etna Volcano Observed by Satellite Radar Interferometry

Riccardo Lanari[1,2], Paul Lundgren[1] and Eugenio Sansosti[1,2]

Jet Propulsion Laboratory, California Institute of Technology, Pasadena, CA 91109, USA

[1]authorship is alphabetical, all authors contributed equally

[2]permanently at IRECE-CNR, 80124 Naples, Italy

Abstract. Satellite radar interferometry of Mt. Etna volcano, Sicily, Italy, reveals a sequence of deformation characterized by deflation during the end of the 1993 eruption, inflation from 1993-1995 with an increase in the inflation rate immediately before its resumed eruptive activity in late 1995. This was followed by very low deformation levels during the following year. The source of the deformation changed from a depth of 9 km during deflation to more than 11-14 km during the subsequent inflation, consistent with a model in which deflation at shallower levels is followed by inflation at greater depth as the volcano system recharges from below before its next eruption. This study demonstrates that radar interferometry provides an important contribution towards understanding the dynamic deformation of volcanoes. By revealing large scale changes in their pre-eruption deformation rates, radar interferometry could play an important role in volcano eruption monitoring.

Introduction

Changes in a volcano's rate and source of deformation provide an important measure of its eruptive potential. Observations of volcano deformation either immediately before or during their eruption have been made with differing spatial and temporal sensitivities . The 1991 eruption of Hekla volcano was detected by strain gauge data over the hours before the eruption [Linde et al., 1993] and by GPS data averaging over more than a year [Sigmundsson et al., 1992]. Differential radar interferometry has already demonstrated its ability to detect a single deflation episode for Mt. Etna [Massonnet et al., 1995]. Conventional geodetic measurements of Etna have been used to measure deformation accompanying dike emplacement [McGuire et al., 1991], with changes in rate of uplift demonstrating the potential to forecast eruptions [Murray et al., 1994].

Here we use the differential radar interferometry technique [Massonnet et al., 1993; Zebker et al., 1994] to reveal the dynamic evolution of a volcano leading up to its eruption. In particular, using European remote sensing satellite (ERS) 1 and 2 data, we observe deformation of Etna volcano (Fig. 1) starting with its deflation during the last flank eruption in 1993, followed by inflation culminating in a surge in uplift prior to renewed activity in 1995. After the resumption in activity in 1995 there was a sudden slowdown in the observed uplift. Modeling the interferometric SAR differential

displacements we find that the depth of the deformation source increased with time: deflation was followed by uplift from a deeper source as deformation changed from deflation to inflation.

SAR Interferometry

We analyzed 18 ERS-1/2 images and generated 19 interferograms from 1992-1996. Fig. 2 shows a selection of these interferograms after removing the topographic contribution derived from a digital elevation model (DEM) [Massonnet et al., 1993]. For this study we use the IIV-CNR DEM for Mt. Etna derived photogrametrically by the Italian Army. This DEM has a 25 m posting, with a height uncertainty of 5-10 m. The resulting differential interferograms are related to the volcano surface deformation in a direction parallel to the radar sensor line of sight. For the ERS-1/2 sensors the line of sight is almost perpendicular to the orbit and has an incidence angle of about 23 degrees for the center of the illuminated scene [ESA, 1992]. All the image pairs selected for this study have a perpendicular baseline component less than 80 meters in order to minimize the topography induced errors [Massonnet and Rabaute, 1995]. For a baseline of 80 m this topographic error would be less than 2.4 mm in range displacement, less than 1/10th of a fringe.

Several deformation features are evident from these interferograms according to the time period spanned by each: 1) During the eruptive period ending in March 1993 the 1992-1993 interferograms show a strong subsidence signal (Fig. 2A). 2) Since 1993 the trend has reversed and interferograms spanning 1993-1995 show a strong inflation signal (Fig. 2B,C). However, the interferogram in Fig. 2B, which ends on April 18, 1995, has noticeably less differential fringes than that in Fig. 2C ending October 10, 1995. 3) Fig. 2D,E shows that from late spring to summer 1995 more than 2 fringes of inflation occurred during the 2 month period spanned by each interferogram. The first of these two ended at the start of resumed eruptive activity on July 30. The second interferogram extends until one month beyond the start of activity. However, the eruptive activity did not achieve its full intensity until November 1995 [Coltelli et al., 1995]. 4) Following the start of volcanic activity we find that interferograms spanning fall 1995 to fall 1996 have low amounts of deformation (Fig. 2F).

Deformation Modeling

Changes in the surface deformation are a reflection of changes in pressure within the volcano

due to variations in magma location and volume. To infer changes in the source of deformation we applied a simple model for surface deformation due to a point source in an elastic half-space. We apply an analytic model [Mogi, 1958] that has been used with much success, despite its limiting assumption of a small pressure source region and no effect of topography. To estimate the effect the latter might have on our depth estimates we also solved for the depth using Mogi functions in which the displacement at each point on the surface was calculated based on its geometric distance from the source [Williams et al., 1997]. We found for all interferograms used in this study that when we used the topographically corrected model we consistently found a depth which was 1 km shallower than for the half-space model. Since the half-space model is more rigorous we chose to use the standard Mogi solution in this study.

In the half-space model the shape of the uplift curve is dependent on the depth of the source, while the properties of the source (change in pressure and cavity radius) are inseparable [McTigue,1987]. To solve for the best point source location we search over a grid of locations for the position and depth which minimizes the misfit between the data and model [Sigmundsson et al., 1992]. For modeling we chose 8 interferograms from 1992-1995, with those from late 1995-1996 having too little amplitude to model as a single point source. For each interferogram the phase was unwrapped to give a continuous measure of the relative displacement in line of sight across the image by using a global phase unwrapping algorithm [Fornaro et al., 1997]. Fig. 3 shows the unwrapped interferograms and the corresponding best fitting models for three different deformation episodes. The unwrapped interferogram in Fig. 3A which spans the eruption ending in 1993 is well fit by a point source at 9 km depth (Fig. 4A). The significantly shallower depth we find compared to a previous interpretation of the same radar image pair [Massonnet et al., 1995] might be due to differences in the generation of the differential interferograms; in particular, we have removed the topographic phase contribution by using the precision orbit data provided by ESA and the aforementioned DEM. However, the 9 km source depth we find is in better agreement with independent observations [Nunnari and Puglisi, 1994; Bonaccorso et al., 1996]. Fig. 3B shows the unwrapped interferogram from August 8, 1993 to October 10, 1995. The uplift pattern we find is elliptical along a NE-SW axis. The best fitting point source does not fully fit the highest uplift areas towards the center (Fig. 4B) and

the elliptical nature of the uplift is further revealed in its residual range displacements (Fig 3B, *bottom*). Fig. 3C shows an unwrapped interferogram from the uplift during the summer of 1995 (Fig. 2E) that is best fit with a point source at 13 km depth.

Discussion

Fig. 5A presents the best fitting point source depths for all eight unwrapped interferograms, showing an increase in depth from deflation to inflation. The increased depth of the deformation pressure source observed during inflation is consistent with refilling of the volcano plumbing system from greater depth. We do not find an upward migration of the deformation source as is commonly expected prior to eruptive activity in 1995, possibly owing to the open nature of Etna's volcanic plumbing system.

Fig. 5B shows a plot of the effective annual uplift rate found for 10 of the analyzed interferograms. Not all of the generated interferograms contributed to the uplift rate analysis since many of them had too great a time separation to be applicable to the present study. For the interferograms from 1993-1995 we are assuming constant deformation in accordance with Global Positioning System (GPS) observations of Etna. Inversion of GPS baseline lengths for the areal dilatation shows that expansion began in early 1993 and was constant through 1994 [Puglisi et al., 1998] and into 1995 [G. Puglisi, personal communication]. The amount of uplift found for the three interferograms from the summer of 1995 are fairly consistent (6.5-8 cm). However, the image pair from April - October 1995 has a lower uplift rate than the much shorter time pairs during the summer. An explanation for this is that most of the inflation during this period occurred within the two months preceding eruption activity. Interferograms from September and October 1995 until June and October 1996, respectively, show little deformation and consequently very low uplift rates. The overall pattern we observe is one of steady inflation following the eruption ending in 1993 with an acceleration in the rate of uplift in the months preceding renewed eruptive activity at the end of July 1995. This is similar to transient uplift observed from leveling measurements on Vulcano volcano prior to subsidence following pressure release due to degassing [Bonafede, 1995].

Whether the renewed eruptive activity in 1995 could have been predicted is difficult to say

given our limited data set. Approaches such as Murray et al. [1994] suggest it may be possible to make rough estimates of impending eruptions if the temporal sampling of the deformation is high enough during the accelerated deformation which occurs before an eruption.

Conclusions

Despite the uneven temporal sampling of the radar images, the dynamic nature of the deformation remains clear. The deflation of Etna during the latter part of the eruption ending in 1993 was replaced by uplift from 1993-1995, culminating with a large increase in the rate of uplift immediately preceding the start of the 1995 eruptive activity. Once activity had resumed there was a distinct reduction in the amount of deformation.

This study shows that satellite radar interferometry is an important tool for understanding the dynamic deformation of volcanoes and that pre-eruptive changes over periods of weeks can be detected. The surge in uplift from mid-crustal depths and the lack of significant deformation from late 1995-1996 is consistent with the sustained eruption that continues to the present.

Acknowledgments: We thank G. Franceschetti (IRECE) for his support. ERS data were provided by the Italian PAF, ASI. We also thank M. Coltelli, G. Peltzer, G. Puglisi, F. Rogez, P. Rosen, M. Simons, and F. Webb, for their critical analysis of this study. R. L. and E. S. were visiting scientists at JPL with a grant from the Italian CNR. This work was done at the Jet Propulsion Laboratory, California Institute of Technology, under contract with NASA.

REFERENCES

Bonafede, M., Interaction between seismic and volcanic deformation: A possible interpretation of ground deformation observed at Vulcano Island (1976-84), *Terra Nova, 7*, 80-86, 1995.

Bonaccorso, A, F. Ferrucci, D. Patane, L. Villari, Fast deformation processes and eruptive activity at Mount Etna (Italy), *J. Geophys. Res., 101*, 17,467-17,480, 1996.

Coltelli, M., M. Pompilio, E. Privitera, S. Spampinato, S. Bonaccorso, and J. L. Moss, Etna (Italy) six lava fountaining episodes from Northeast crater, *Smithsoniam Inst. Bull. Global Volcanism Network, 20*, 1995.

Elachi, C., Spaceborne radar remote sensing: Applications and techniques, IEEE Press, New York,

254 pp., 1988.

European Space Agency, ERS-1 System, ESA Publications Division, ESTEC, Noordwijk, Netherlands, 1992.

Fornaro, G., G. Franceschetti, R. Lanari, D. Rossi, and M. Tesauro, Interferometric SAR phase unwrapping via the finite element method, *IEE Proc. Radar, Sonar, Navigation, 144*, 226, 1997.

Linde, A. T., K. Agustsson, I. S. Sacks, and R. Stefansson, Mechanism of the 1991 eruption of Hekla from continuous borehole strain monitoring, *Nature, 365*, 737-740, 1993.

Massonnet, D., M. Rossi, C. Carmona, F. Adragna, G. Peltzer, K. Feigl, and T. Rabaute, The displacement field of the Landers earthquake mapped by radar interferometry, *Nature, 364*, 138-142, 1993.

Massonnet, D., and T. Rabaute, Radar interferometry: Limits and potential, *IEEE Trans Geosci. Rem. Sensing, 31*, 455, (1993).

Massonnet, D., P. Briole, and A. Arnaud, Deflation of Mount Etna monitored by spaceborne radar interferometry, *Nature, 375*, 567-570, 1995.

McGuire, W. J., J. B. Murray, A. D. Pullen, and S. J. Saunders, Ground deformation monitoring at Mt. Etna; evidence for dyke emplacement and slope instability, *J. Geol. Soc. London, 148*, 577-583, 1991.

McTigue, D. F., Elastic stress and deformation near a finite spherical magma body: Resolution of the point source paradox, *J. Geophys. Res., 92*, 12,931-12,940, 1987.

Mogi, K., Relations between the eruptions of various volcanoes and the deformations of the ground surfaces around them, *Bull. Earthquake Res. Inst. Tokyo, 36*, 99-134, 1958.

Murray, J. B., B. Voight, and J. -P. Glot, Slope movement crisis on the east flank of Mt. Etna volcano: Models for eruption triggering and forecasting, *Eng. Geol., 38*, 245-259, 1994.

Nunnari, G., and G. Puglisi, The Global Positioning System as a useful technique for measuring ground deformationd in volcanic areas., *J. Volcanol. Geotherm. Res., 61*, 267-280, 1994.

Puglisi, G., A. Bonforte, and S. R. Maugeri, Ground deformation patterns on Mt. Etna, between 1992 and 1994, inferred from GPS data, *Bull. Volcanol.*, submitted, 1998.

Sigmundsson, F., P. Einarsson, and R. Bilham, Magma chamber deflation recorded by the Global Positioning System: The Hekla 1991 eruption, *Geophys. Res. Lett.*, *19*, 1483-1486, 1992.

Williams, C. A., N. F. Stevens, G. Wadge, J. G. Morley, J. -P. Muller, M. Upton, and J. B. Murray, Numerical modeling of the deformation field at Mt. Etna volcano, Sicily, constrained by interferometry and GPS measurements, *EOS Trans. Amer. Geophys. Un., Fall Meeting Suppl., 78*, F798, 1997.

Zebker, H. A., P. A. Rosen, R. M. Goldstein, A. G. Gabriel, C. L. Werner, On the derivation of coseismic displacement fields using differential radar interferometry: The Landers earthquake, *J. Geophys. Res. 99,* 19,617-19,634, 1994.

Zebker, H. A., P. A. Rosen, and S. Hensley, Atmospheric effects in interferometric synthetic aperture radar surface deformation and topographic maps, *J. Geophys. Res. 102*, 7547-7563, 1997.

Figure Captions

Fig. 1. Location of Etna volcano in NE Sicily, Italy (inset), and the contoured (300 m intervals) digital elevation model used to remove the topographic component from the differential interferograms.

Fig. 2. Selected differential interferograms from Mt. Etna in Universal Transverse Mercator projection. Each fringe represents a change in phase corresponding to about 2.8 cm of displacement in line of sight. (A) 92/9/27_93/10/17, where the dates represent the acquisition dates of the first and second ERS radar image, respectively. The perpendicular component of the spatial baseline between the two acquisitions (B⊥) equals 32m. (B) 93/8/8_95/4/18, B⊥=31m. (C) 93/8/8_95/10/10, B⊥=59m. (D) 95/5/24_95/8/2, B⊥=59m. (E) 95/6/27_95/9/5, B⊥=40m. (F) 95/10/10_96/10/30, B⊥=1m.

Fig. 3. Comparison of three unwrapped interferograms and their best fitting point source model for deflationary and inflationary phases. (A) Line of sight displacements from the interferogram of 92/9/27_93/10/17 where the thin vertical line marks the location of the corresponding profile in Fig. 4. (*top*) Unwrapped interferogram. (*middle*) Best fitting model. (*bottom*) Residual between the data and the best fitting model. (B) are the same as in (A) but for the interferogram of 93/8/8_95/10/10. (C) are the same as in (A) but for the interferogram of 95/6/27_95/9/5. The black zone approximately in the center of the images represents the topographic layover area that has been excluded because it does not contain information due to the SAR signal under-sampling effect [Elachi, 1988].

Fig. 4. North-South cross sections through the respective observed and modeled radar line-of-sight displacements shown in Fig. 3. The solid gray line is the observed displacement, the dashed line is the model. The letters correspond to the letters assigned in Fig. 3.

Fig. 5. (A) Best fitting depth for the 8 unwrapped interferograms modeled in this study. The filled circle gives the depth located in time at the mid-point between the image pair. The vertical line through each circle marks the standard deviation in the depth estimate. The vertical arrows mark the end of eruptive activity in 1993 and the start of renewed activity in 1995. (B) Uplift rate for each interferogram. The (+) symbol represents the middle of the interferogram time span. The rate is based on the observed interferogram relative uplift divided by its time span. We plot each as a box where the

height of the box is based on an assumed uncertainty of 1/2 fringe (corresponding to 1.4 cm) in line of sight displacement, mostly due to atmospheric delay [Massonnet et al., 1995; Zebker et al., 1997]; the length of the box corresponds to the time spanned by the image pair.

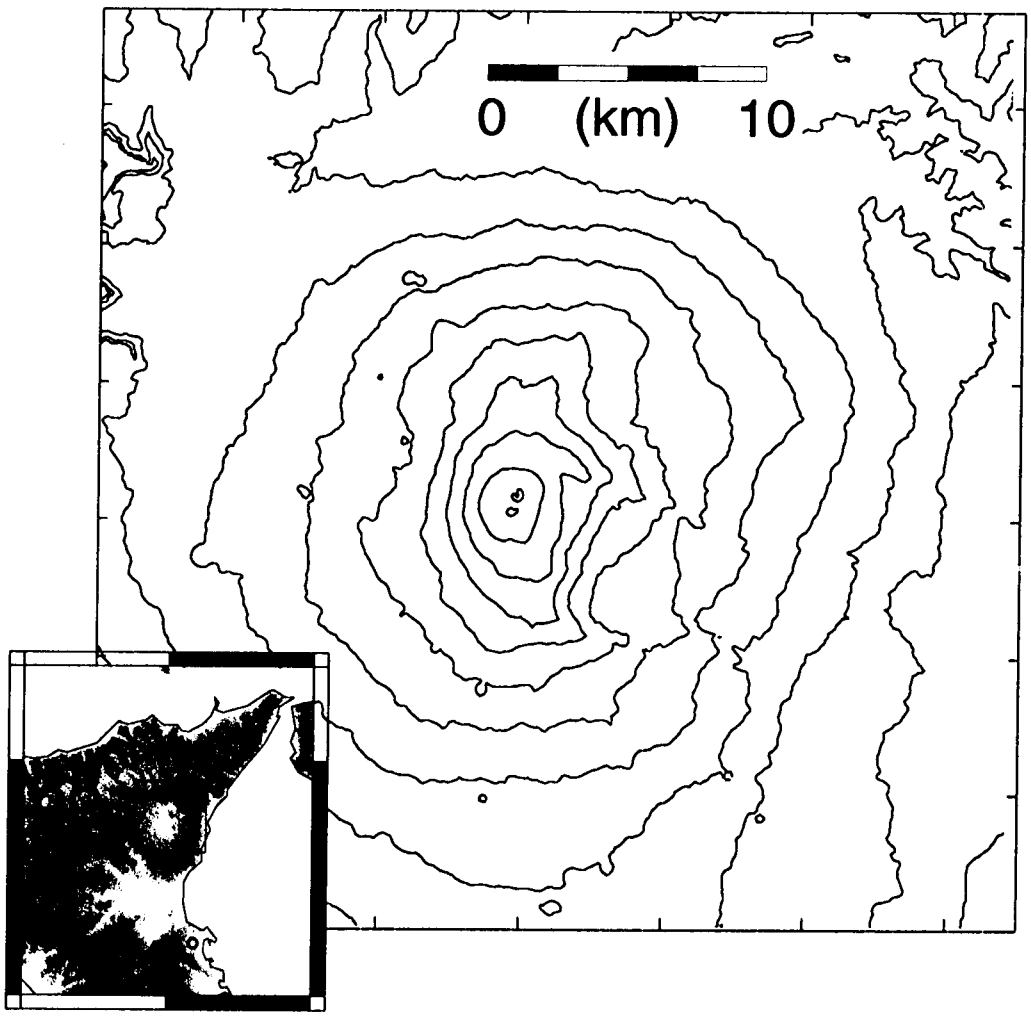

Figure 1

R. Lanari, P. Lundgren, E. Sansosti

R. Lanari, P. Lundgren, E. Sansosti, 1997

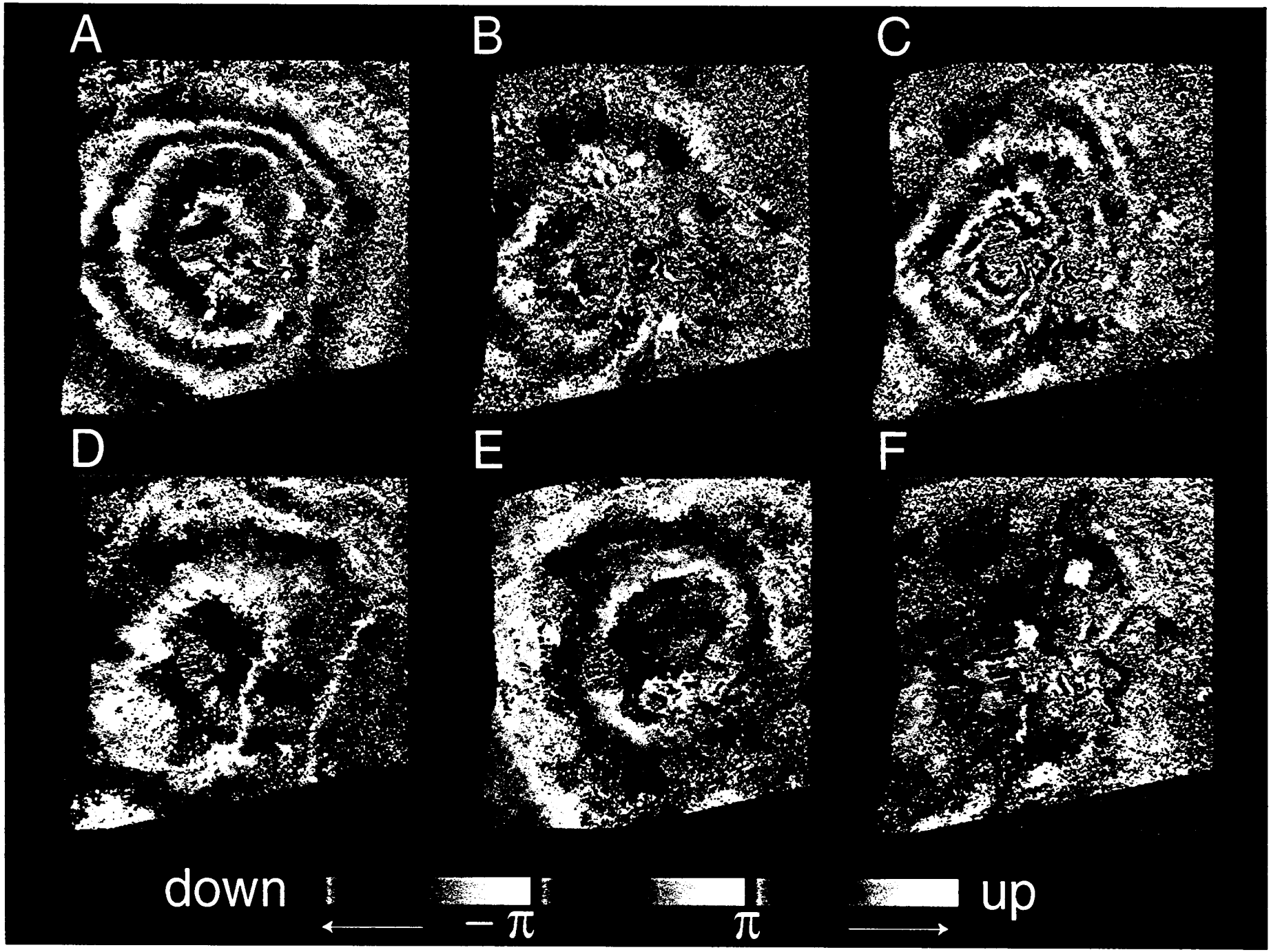

Figure 2

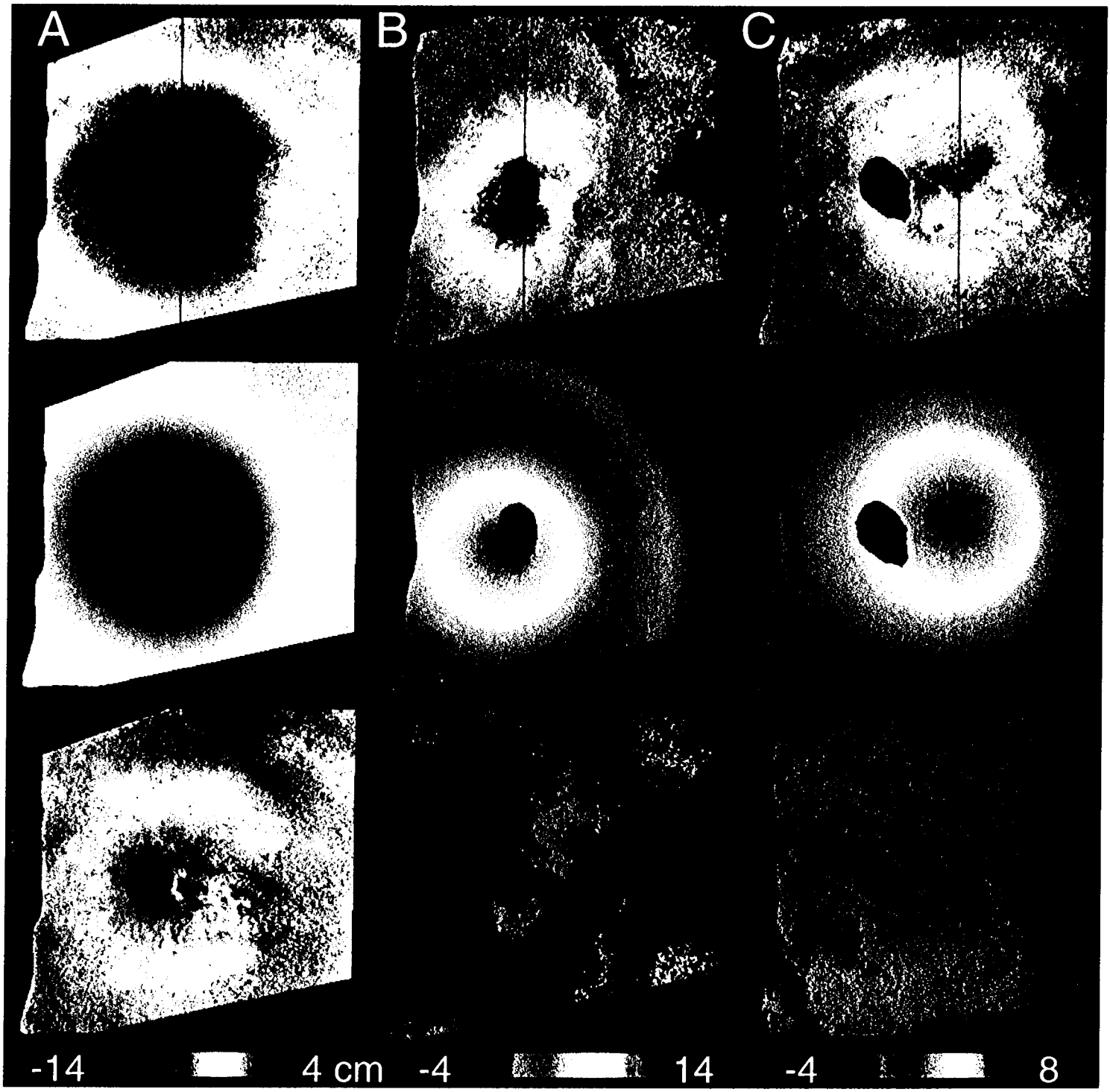

Figure 3.

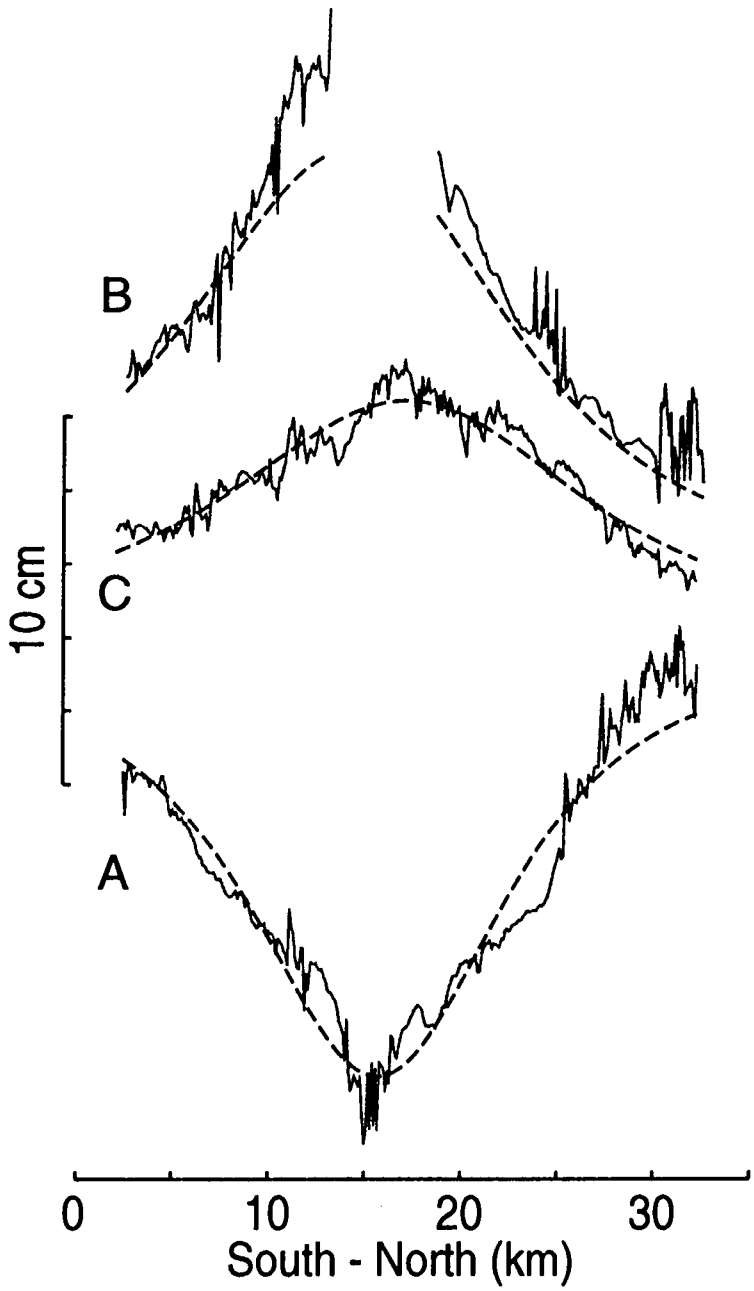

Figure 4.

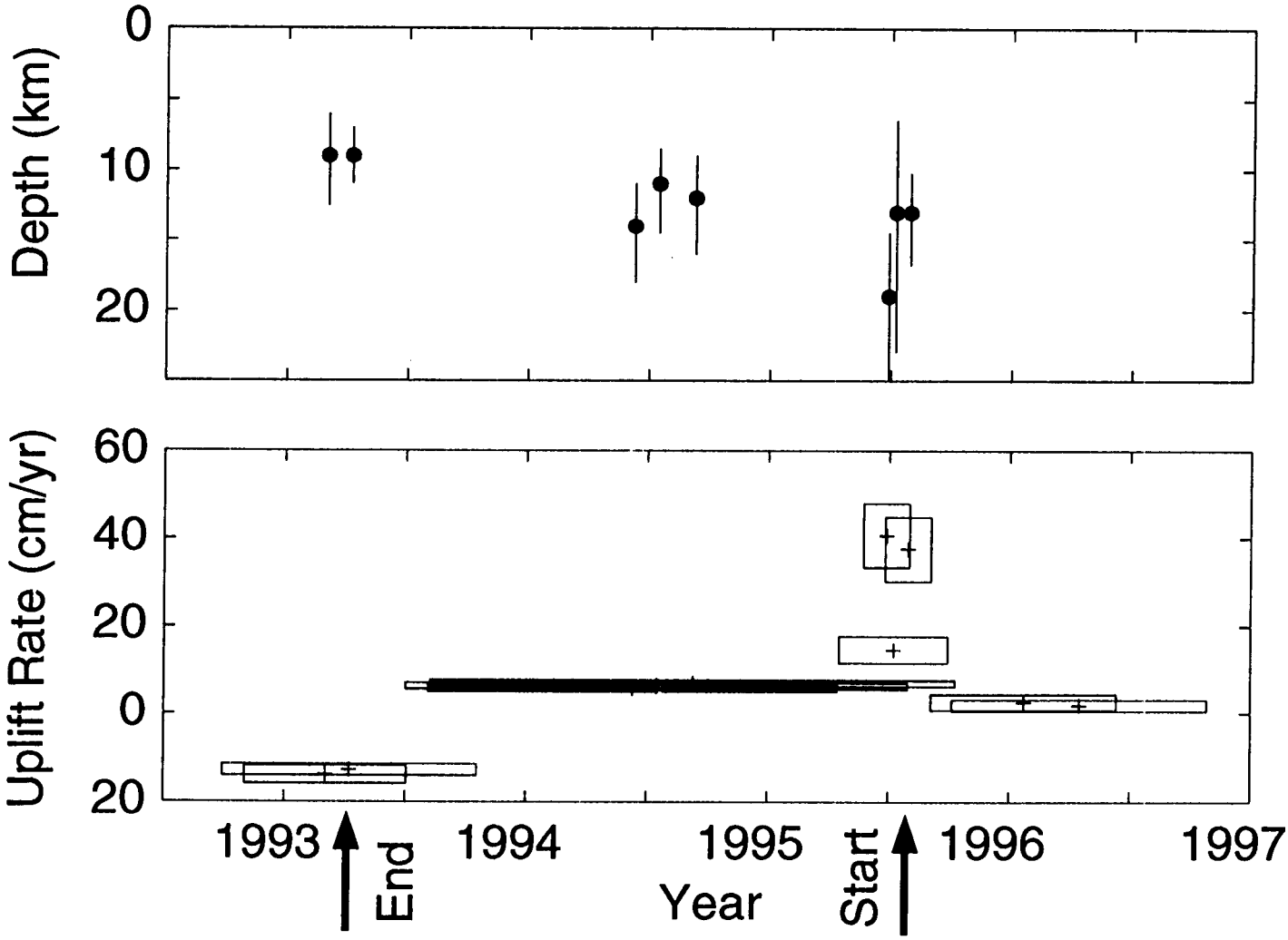
Depth (km)
0
10
20
Uplift Rate (cm/yr)
60
40
20
0
20
1993
End
1994
1995
Year
Start
1996
1997

Figure 5